MATHEMATICAL MODELLING
МАТЕМАТИЧЕСКОЕ МОДЕЛИРОВАНИЕ

CC BY

Check for updates

UDC 519.6

Original Empirical Research

https://doi.org/10.23947/2587-8999-2025-9-4-22-37

Unsteady Model of Blood Coagulation in Aneurysms of Blood Vessels

Natalya K. Volosova[1], Konstantin A. Volosov[2], Aleksandra K. Volosova[2], Mikhail I. Karlov[3], Dmitriy F. Pastukhov[4] ✉, Yuriy F. Pastukhov[4]

[1] MGTU named after. N.E. Bauman, Moscow, Russian Federation

[2] Russian University of Transport, Moscow, Russian Federation

[3] Moscow Institute of Physics and Technology (National Research University), Dolgoprudny, Russian Federation

[4] Polotsk State University named after Euphrosyne of Polotsk, Novopolotsk, Republic of Belarus

✉ dmitrij.pastuhov@mail.ru

Abstract

Introduction. A two-dimensional hydrodynamic problem is numerically solved in the "stream function-vorticity" formulation for an open rectangular cavity simulating blood flow and its coagulation within a vascular aneurysm. The model accounts for a simplified nonlinear mathematical description of the first phase of blood coagulation (30 seconds).

Materials and Methods. To accelerate the numerical solution of the unsteady problem with an explicit finite-difference scheme for the vorticity dynamics equation, an n-fold splitting method of the explicit scheme ($n = 100, 200$) was employed, along with the use of a symmetry plane in the rectangular aneurysm domain. The splitting method was also applied to solve the dynamic system of advection–diffusion equations with nonlinear source terms for the activator and inhibitor blood factors ($N = 70$). The maximum time step τ_0 was synchronized across both splitting cycles. The computation was performed on half of the rectangular aneurysm using a uniform 100×50 grid with equal spacing $h_1 = h_2 = 0.01$. The inverse matrix required for solving the Poisson equation in the "stream function-vorticity" formulation with a finite number of elementary operations was computed using the Msimsl library.

Results. The numerical solution demonstrated that, in arterioles (Re = 3.6), advection and diffusion of fibrin occur according to the nonlinear dynamics of activator and inhibitor factors, as if fibrin were moving counter to the blood flow. The maximum fibrin density forms in the central region of the vessel in the shape of a "fibrin horseshoe". For higher Reynolds numbers (Re = 3000) corresponding to arteries, fibrin motion occurs along the main flow, and the central part of the vessel is separated from the aneurysm by a "fibrin foot" along its geometric boundary. In arterioles, a layered fibrin growth effect was also observed, with periodic variations in fibrin density near the aneurysm wall, consistent with other authors' findings. In arteries, the fibrin film within the aneurysm forms in approximately one second—significantly shorter than the first coagulation phase (30 seconds).

Discussion. The finite-difference approximation achieves sixth-order accuracy at interior nodes and fourth-order accuracy at boundary nodes. The model was applied to simulate blood flow in arterial aneurysms at high Reynolds numbers (Re = 3000) and in arteriole aneurysms (Re = 3.6). The dimensionless range of fibrin density variation is consistent with data reported by other researchers.

Conclusions. The study proposes a system of equations representing a simplified unsteady model of blood motion and fibrin (thrombus) formation in vascular aneurysms. The proposed model provides a qualitative understanding of thrombus formation mechanisms in aneurysms of arteries and arterioles, as well as in elements of medical equipment.

Keywords: hydrodynamics, numerical methods, partial differential equations, initial-boundary value problem, mathematical modeling, aneurysm

For Citation. Volosova N.K., Volosov K.A., Volosova A.K., Karlov M.I., Pastukhov D.F., Pastukhov Yu.F. Unsteady Model of Blood Coagulation in Aneurysms of Blood Vessels. *Computation Mathematics and Information Technologies*. 2025;9(4):22–37. https://doi.org/10.23947/2587-8999-2025-9-4-22-37

 © *Volosova N.K., Volosov K.A., Volosova A.K., Karlov M.I., Pastukhov D.F., Pastukhov Yu.F., 2025*

Оригинальное эмпирическое исследование

Нестационарная модель свертывания крови в аневризмах кровеносных сосудов

Н.К. Волосова[1], К.А. Волосов[2], А.К. Волосова[2], М.И. Карлов[3], Д.Ф. Пастухов[4] ✉, Ю.Ф. Пастухов[4]

[1] Московский государственный технический университет им. Н.Э. Баумана, г. Москва, Российская Федерация

[2] Российский университет транспорта, г. Москва, Российская Федерация

[3] Московский физико-технический институт (национальный исследовательский университет), г. Долгопрудный, Российская Федерация

[4] Полоцкий государственный университет им. Евфросинии Полоцкой, г. Новополоцк, Республика Беларусь

✉ dmitrij.pastuhov@mail.ru

Аннотация

Введение. Численно решается двумерная гидродинамическая задача в переменных «функция тока — вихрь» в открытой прямоугольной каверне, моделирующей течение крови и ее свертывание в аневризме кровеносного сосуда с учетом простейшей нелинейной математической модели за время первой фазы свертывания (30 секунд).

Материалы и методы. Для ускорения численного решения нестационарной задачи с явной разностной схемой уравнения динамики вихря использовался метод n-кратного расщепления явной разностной схемы (n = 100, 200) и наличие плоскости симметрии прямоугольной области каверны — аневризмы. Метод расщепления также применялся для решения динамической системы уравнений адвекции-диффузии с нелинейной правой частью для факторов крови активатора и ингибитора (N = 70). В двух методах согласовался максимальный шаг времени τ_0 в циклах расщепления. На половине прямоугольной аневризмы рассматривались симметричные решения и применялась равномерная сетка 100×50 с равным шагом $h_1 = h_2 = 0{,}01$. Обратная матрица для решения уравнения Пуассона в переменных «функция тока — вихрь» за конечное число элементарных операций вычислялась библиотекой Msimsl.

Результаты исследования. Численное решение задачи показало, что в артериолах (Re = 3,6) происходит адвекция и диффузия фибрина с учетом нелинейной правой части системы уравнений динамики для активатора и ингибитора так, как если бы фибрин двигался навстречу крови. Максимальная плотность фибрина реализуется в средней части сосуда в форме «фибриновой подковы». Решение задачи при больших числах Рейнольдса (Re = 3000) в артериях эквивалентно движению фибрина вдоль потока, при этом центральная часть кровеносного сосуда отделена от аневризмы по ее геометрической границе «фибриновой ножкой». В артериолах обнаружен также эффект слоеного роста фибрина с периодическим изменением плотности у стенки аневризмы, как и у авторов других работ. Решение задачи в артерии показало, что фибриновая пленка в аневризме при быстром движении крови образуется за время порядка одной секунды, что много меньше, чем первая фаза свертывания (30 секунд).

Обсуждение. Аппроксимация уравнений имеет шестой порядок погрешности во внутренних узлах и четвертый в граничных узлах. Задача решена для движения крови в аневризмах артерий при больших числах Рейнольдса (Re = 3000) и для течения крови в аневризмах артериол (Re = 3,6). Безразмерный диапазон изменения плотности фибрина вкладывается в аналогичный диапазон в работах других авторов.

Заключение. В работе предложены системы уравнений, представляющие собой простейшую нестационарную модель движения крови и образования фибрина (тромба) в аневризмах кровеносных сосудов. Предложенная модель поможет качественно выяснить причины образования тромбов в аневризмах артерий и артериол, а также в элементах медицинского оборудования.

Ключевые слова: гидродинамика, численные методы, уравнения в частных производных, начально-краевая задача, математическое моделирование, аневризма

Для цитирования. Волосова Н.К., Волосов К.А., Волосова А.К., Карлов М.И., Пастухов Д.Ф., Пастухов Ю.Ф. Нестационарная модель свертывания крови в аневризмах кровеносных сосудов. *Computational Mathematics and Information Technologies*. 2025;9(4):22–37. https://doi.org/10.23947/2587-8999-2025-9-4-22-37

Introduction. This study, which continues the research presented in [1], for the first time models a two-dimensional hydrodynamic problem of blood motion and coagulation in an open rectangular aneurysm-cavity using the “stream function — vorticity” formulation. In [2], a system of two dynamic partial differential equations describing the diffusion of coagulation factors-activator and inhibitor — was first derived, with nonlinear source terms accounting for the local interaction between these factors. In [3], several mathematical models of blood coagulation without advection were compared, and the dimensional coefficients in the governing equations were refined.

The dynamics of blood formation and its relation to cardiac pulsations at low Reynolds numbers were investigated in [4]. In [5], blood motion in an arteriole was studied using the Russian computational platform FlowVision, incorporating intermediate components of chemical reactions and accounting for variations in both the solid boundary of the vessel and the thrombus interface. It was shown that small thrombi form near an internal cut within a straight vessel and exhibit a fractal structure. Studies [6–11] focus on two-dimensional hydrodynamic problems whose properties are similar to those of the present hydrodynamic system.

The present work, firstly, introduces an unsteady mathematical model of blood coagulation within a vascular aneurysm for both an arteriole (Re = 3.6) and an artery under turbulent conditions (Re = 3000). Secondly, the developed computational algorithm incorporates the periodic mixing of blood within the aneurysm caused by each pulsation wave.

Materials and Methods

Problem Statement. We consider a two-dimensional problem of blood flow and coagulation in a rectangular aneurysm–cavity formed on the wall of a blood vessel. The aneurysm represents a section of the vessel whose diameter $2d$ is typically twice that of the main vessel. Let L denote the aneurysm length, $2H$ its diameter, and H the half-width of the aneurysm (Fig. 1 illustrates half of the symmetric model). The variable d represents the half-width of the parent vessel. The origin of the coordinate system is placed at the lower left corner of the computational domain.

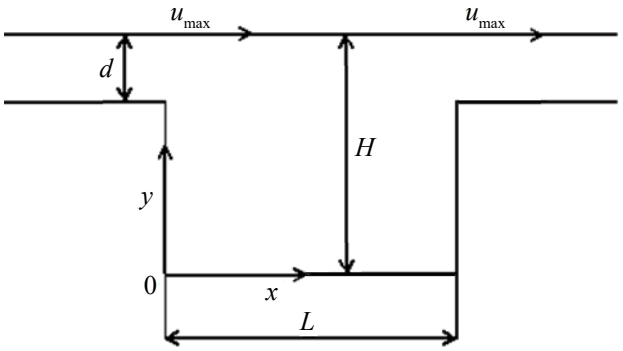

Fig. 1. Geometry of the computational domain for the numerical solution

The dynamic part of the problem describing blood motion in aneurysms of arterioles (Re = 1.8) and arteries (Re = 1500) was numerically solved in [1]. That study obtained the streamline patterns of fluid (blood) particles inside the aneurysm. The formulation of the hydrodynamic problem in [1] in dimensionless variables has the following form:

$$\begin{cases} \bar{\psi}_{\bar{x}\bar{x}} + \bar{\psi}_{\bar{y}\bar{y}} = -\bar{w}(\bar{x},\bar{y}),\ 0 < \bar{x} = \dfrac{x}{L} < 1,\ \ 0 < \bar{y} < k_{\max}, \\ \bar{w} = \bar{v}_{\bar{x}} - \bar{u}_{\bar{y}}, \\ \bar{u} = \bar{\psi}_{\bar{y}}; \bar{v} = -\bar{\psi}_{\bar{x}}, \\ \bar{w}_{\bar{t}} + \bar{u}\cdot\bar{w}_{\bar{x}} + \bar{v}\cdot\bar{w}_{\bar{y}} = \dfrac{1}{\mathrm{Re}}\left(\bar{w}_{\bar{x}\bar{x}} + \bar{w}_{\bar{y}\bar{y}}\right), 0 < \bar{t} = \dfrac{t}{T}, \\ \bar{\psi}\big|_{\Gamma 1} \equiv 0, \bar{v}\big|_{\Gamma} \equiv 0, \bar{u}\big|_{\Gamma_1} = 0, \bar{v}\big|_{\Gamma_2} = 0, \\ \psi(0,y) = \psi(L,y) = \begin{cases} 0, y \in [0, H-\Delta], \\ u_{\max} L\left(\dfrac{y}{L} + \dfrac{2}{3}\dfrac{\Delta}{L} - \dfrac{H}{L} - \dfrac{\left(y/L - H/L\right)^3}{3\left(\Delta/L\right)^2}\right), y \in [H-\Delta, H], \\ \dfrac{2}{3}u_{\max}\Delta, y = H. \end{cases} \end{cases} \quad (1)$$

As in [1], the following characteristic scales are used in this study: length — L, time — $\dfrac{L}{u_{\max}}$, velocity — $u_{\max}$, stream function — $Lu_{\max}$, vorticity — $\dfrac{u_{\max}}{L}$, and Reynolds number — Re. Let us introduce the dimensionless variables: $\bar{x}$ — horizontal coordinate, $\bar{y}$ — vertical coordinate, $\bar{\psi}$, $\bar{w}$ — stream function and vorticity, respectively, $(\bar{u}, \bar{v})$ — velocity vector, $\bar{t}$ — time. They are defined by the relations:

$$0 \le \bar{x} = \frac{x}{L} \le 1,\ \ 0 \le \bar{y} = \frac{y}{L} \le k = \frac{H}{L}, \bar{\psi} = \frac{\psi}{\psi_{\max}}, \psi_{\max} = Lu_{\max},$$

$$\bar{u}=\frac{u}{u_{\max}},\bar{v}=\frac{v}{u_{\max}}\bar{w}=\frac{w}{w_{\max}},w_{\max}=\frac{u_{\max}}{L},$$
$$\bar{t}=\frac{t}{T},T=\frac{L}{u_{\max}},\mathrm{Re}=\frac{u_{\max}L}{\nu}.$$

The kinematic viscosity of blood is taken as $\nu=\frac{\mu}{\rho}=\frac{3.5\cdot10^{-3}\,\mathrm{Pa\cdot s}}{1050\ \mathrm{kg/m^3}}=3.33(3)\cdot10^{-6}\,\frac{\mathrm{m}^2}{\mathrm{s}}$.

In system (1), the first equation represents the Poisson equation in the "stream function–vorticity" formulation, approximated with sixth-order accuracy according to [12] and [1]:

$$\Delta\psi=\psi_{xx}+\psi_{yy}=f(x,y)=-w\Leftrightarrow\frac{1}{h^2}\left(-\frac{10}{3}\psi_{0,0}+\frac{2}{3}\left(\psi_{-1,0}+\psi_{0,-1}+\psi_{1,0}+\psi_{0,1}\right)+\frac{1}{6}\left(\psi_{-1,-1}+\psi_{1,-1}+\psi_{-1,1}+\psi_{1,1}\right)\right)=$$
$$=f+\frac{h^2}{12}\left(f_{xx}+f_{yy}\right)+\frac{h^4}{360}\left(f_x^{(4)}+f_y^{(4)}\right)+\frac{h^4f_{xxyy}^{(4)}}{90}+O\left(h^6\right)=-\left(w+\frac{h^2}{12}\left(w_{xx}+w_{yy}\right)+\frac{h^4}{360}\left(w_x^{(4)}+w_y^{(4)}\right)+\frac{h^4w_{xxyy}^{(4)}}{90}\right)+O\left(h^6\right). \quad (2)$$

The partial derivatives in formula (2) were also approximated in [1]. Finite-difference expressions were obtained for the interior nodes of the function f with indices $n=\overline{2,n_1-2},m=\overline{2,n_2-2}$:

$$\begin{cases}f_{xx}+f_{yy}=\frac{1}{h^2}\left(-5f_{0,0}+\frac{4}{3}\left(f_{-1,0}+f_{0,-1}+f_{1,0}+f_{0,1}\right)-\frac{1}{12}\left(f_{-2,0}+f_{0,-2}+f_{2,0}+f_{0,2}\right)\right)+O\left(h^4\right),\\ f_x^{(4)}+f_y^{(4)}=\frac{1}{h^4}\left(12f_{0,0}-4\left(f_{-1,0}+f_{0,-1}+f_{1,0}+f_{0,1}\right)+f_{-2,0}+f_{0,-2}+f_{2,0}+f_{0,2}\right)+O\left(h^2\right),\\ f_{xxyy}^{(4)}=\frac{1}{h^4}\left(4f_{0,0}-2\left(f_{-1,0}+f_{0,-1}+f_{1,0}+f_{0,1}\right)+f_{-1,-1}+f_{-1,1}+f_{1,-1}+f_{1,1}\right)+O\left(h^2\right).\end{cases} \quad (3)$$

The combined algorithm for solving system (1) together with system (12) consists of 11 computational steps. It requires the specification of initial conditions for the following variables: the stream function field, velocity field, vorticity field, and the inhibitor and activator concentration fields (equations (15)–(17)).

This algorithm differs from that presented in [1] and can be summarized as follows:

Step 1: Define the boundary conditions on the rectangular cavity contour for the stream function and for the vertical velocity component, which remain constant throughout the computation.

Step 2: Modify the right-hand side of the Poisson equation for the vorticity according to formulas (12) and (13) from [1].

Step 3: Solve the Poisson equation (7)–(11) from [1], i. e., compute the stream function values at the interior grid points of the rectangular domain.

Step 4: Compute the velocity along the upper segment of the cavity using formulas (5) from [1].

Step 5: Evaluate the updated velocity field using equation (18) from [1] at the interior grid nodes.

Step 6: Determine the new boundary values of vorticity using formulas (24) from [1].

Step 7: Compute the new vorticity values at the interior grid nodes using equation (19) from [1].

Step 8: Evaluate the right-hand sides for the inhibitor and activator equations (13).

Step 9: Solve equation (13) separately for the inhibitor and for the activator using the splitting method at the interior grid nodes.

Step 10: Determine the boundary values of the inhibitor and activator according to formula (14).

Step 11: If the physical time corresponds to an integer number of cardiac pulsations, reset the velocity, stream function, and vorticity fields to their initial values before solving equation (17). This procedure simulates blood mixing inside the aneurysm induced by a pulsation wave generated by the heart along the vessel system. The inhibitor, activator, and fibrin fields remain unchanged before and after the pulsation.

After completing the tenth step, the algorithm returns to the first step in a cyclic manner. In system (1), the Poisson equation is solved first, requiring a finite number of elementary operations [1] and providing sixth-order accuracy at the interior grid nodes. The second equation in system (1) corresponds to the vorticity function, which is computed through the coordinate derivatives of the velocity field.

The third equation expresses the velocity components as partial derivatives of the stream function. Therefore, the approximation of these equations $\bar{w}=\bar{v}_{\bar{x}}-\bar{u}_{\bar{y}},\bar{u}=\bar{\psi}_{\bar{y}};\bar{v}=-\bar{\psi}_{\bar{x}}$ reduces to approximating first derivatives, which poses no particular difficulty. The fourth equation in system (1) represents the vorticity dynamics equation—the only equation in the system that explicitly depends on time. The left-hand side contains the total (convective) time derivative.

In system (1), the elements of the rectangular cavity boundary must be clarified. Here, $\Gamma 1$ denotes the union of the lower parts of the lateral sides and the bottom segment, while $\Gamma 2$ corresponds to the upper boundary of the rectangle Γ. Let

($u(x,u)$, $v(x,y)$) denote the velocity vector of a fluid particle. On the solid boundary — that is, along the bottom segment and the lower parts of the lateral sides of height $H–d$ of the rectangular cavity — the velocity is zero (the no-slip condition on $\Gamma 1$). Accordingly, the stream function is set to zero along this boundary.

On the upper boundary of the rectangle, the vertical velocity component is zero, while the horizontal component is not specified on the upper segment and is zero on the bottom segment. On the lateral sides, it is described by equation (4) according to [1]:

$$\bar{u}(0,y)=\bar{u}(L,y)=\frac{u(y)}{u_{\max}}=\begin{cases}0, y\in[0,H-\Delta]\\ \left(1-\dfrac{(y-H)^2}{\Delta^2}\right), y\in[H-\Delta,H].\end{cases} \tag{4}$$

In the upper segment of the rectangular cavity, the unknown velocity can be determined using formulas (5), which correspond to the fourth step of the general algorithm described in [1]:

$$u(n_2,j)=\psi_y(n_2,j)=\frac{1}{(-h_2)}\left(-\frac{83711}{27720}\psi_{n_2,j}+11\psi_{n_2-1,j}-\frac{55}{2}\psi_{n_2-2,j}+55\psi_{n_2-3,j}-\frac{165}{2}\psi_{n_2-4,j}+\frac{462}{5}\psi_{n_2-5,j}-\right.$$
$$\left.-77\psi_{n_2-6,j}+\frac{330}{7}\psi_{n_2-7,j}-\frac{165}{8}\psi_{n_2-8,j}+\frac{55}{9}\psi_{n_2-9,j}-\frac{11}{10}\psi_{n_2-10,j}+\frac{1}{11}\psi_{n_2-11,j}\right)+O\left(h^{10}\right), j=\overline{1,n_1-1}, \tag{5.1}$$

$$u(n_2,j)=\frac{1}{(-h_2)}\left(-\frac{137}{60}\psi_{n_2,j}+5\psi_{n_2-1,j}-5\psi_{n_2-2,j}+\frac{10}{3}\psi_{n_2-3,j}-\frac{5}{4}\psi_{n_2-4,j}+\frac{1}{5}\psi_{n_2-5,j}\right)+O\left(h^4\right), j=\overline{1,n_1-1}. \tag{5.2}$$

To accelerate the numerical computation, due to the symmetry of the geometry, we consider one half of the aneurysm and two halves of the rectangular channels supplying and discharging the fluid from the aneurysm. It is convenient to introduce a rectangular coordinate system with a uniform grid $n_1 \times n_2 = 100\times 50$.

According to the projection principle, for two convex closed contours nested within each other without self-intersections (contact or partial coincidence of contours is allowed), a ray can be drawn from a certain internal point intersecting each contour at exactly one point. In this case, one may speak of geometric projection of one contour onto another.

Similarly, the projection of a physical field can be defined by transferring the field value at a point on the outer contour to the corresponding point on the inner contour. For example, in Fig. 1, the outer contour includes the left and right parts of the blood vessel and the rectangular aneurysm, whereas the inner contour consists only of the aneurysm. The projection of the outer contour points can also be performed along the normal direction onto the inner contour.

Thus, based on the field projection principle, the problem can be simplified, and its numerical solution significantly accelerated by considering the fluid motion only within the aneurysm domain, rather than within the combined volumes of the three bodies (the left vessel part, the aneurysm, and the right vessel part).

Therefore, it is assumed that the velocity profile is preserved when the flow enters the rectangular aneurysm and when it exits through a narrow symmetric strip with respect to the $0xz$-plane of width $2\Delta = 2d$, where at infinity the velocity distribution is described by the Poiseuille formula (4) [1].

By integrating formula (4) over the interval $y\in[H-\Delta, H]$ we obtain the stream function on the lateral sides of the aneurysm — the last expression in the system of equations (1) [1]. On the upper and lower segments of the aneurysm, as well as on the small adjacent side segments, projection of the velocity field and stream function is not required.

The field projection principle can be qualitatively justified using the classical example of the flow of an ideal fluid around an infinite cylinder. If the velocity field of the ideal fluid at infinity is constant, then at the diametrically opposite points of the cylinder the flow direction remains unchanged, while the velocity magnitude is doubled. At the same time, at the contact points and in the neighboring regions, the no-penetration condition on the cylinder surface is approximately satisfied.

Similarly, in Fig. 1, on the plane of symmetry, the flow direction remains unchanged; the direction of the velocity vector on the lateral inflow and outflow segments of the aneurysm connected to the blood vessel also remains approximately constant. The no-penetration condition of rigid boundaries is thus fulfilled approximately, which justifies the application of the field projection principle on the lateral sides of the aneurysm.

To accelerate the numerical solution of the vorticity equation (1), the splitting method was employed [1, 11]. Analytically, the method of n-fold splitting of the vorticity equation for the time interval τ_0/n can be expressed as follows:

$$\frac{w^{k+((i+1)/n)}-w^{k+(i/n)}}{\tau_0/n}+u^k\cdot w_x^{k+(i/n)}+v^k\cdot w_y^{k+(i/n)}=\frac{1}{\mathrm{Re}}\left(w_{xx}^{k+(i/n)}+w_{yy}^{k+(i/n)}\right), i=\overline{0,n-1}. \tag{6}$$

The system of recurrent equations (6) for the vorticity with a frozen velocity field $\left(u^k(x,y),v^k(x,y)\right), i=\overline{0,n-1}$, $k=const, k=1,2,...$ consists of n intermediate steps $i=\overline{0,n-1}$, the superscript i denotes the number of the intermediate

time layer in the vorticity equation (6), while the subscript k corresponds to the multiple time layer index in system (6). The velocity and stream function fields remain constant in equations (6) for fixed values of $k = const$ and varying index $i = \overline{0, n-1}$. Within this system, only the vorticity field $w^{k+(i/n)}, i = \overline{0, n-1}$ evolves. The velocity field undergoes a discrete change in system (1) when the temporal index of the vorticity function increases by one, from k to $k + 1$ in equations (6).

The main idea of the splitting scheme for system (6) lies in reducing both rounding error accumulation and computational time during the numerical solution. The differential operators with respect to spatial coordinates in (6) are approximated at internal grid nodes with accuracy $O(h^6)$, consistent with all equations in system (1); the boundary conditions are approximated with accuracy $O(h^4)$, and the temporal derivatives — with accuracy $O(\tau)$.

Here, we rely on an unproven but commonly accepted assumption that, for spectral time stability of finite-difference schemes, the approximation order of the equations on the boundary must be lower than that in the internal grid nodes [12]. Thus, over the time interval τ_0/n ((associated with a local decrease in solution stability caused by singular points in the velocity field), solving equation (6) n times yields a temporal jump τ_0 which is n times larger than that obtained by the sequential solution of system (1).

For the derivative w_y in (6), the quadrature formulas are written as follows (the formulas for w_x are analogous):

$$\begin{cases} w_{y(i,j)} = \frac{1}{h}\left(\frac{3}{4}\left(w_{i+1,j} - w_{i-1,j}\right) - \frac{3}{20}\left(w_{i+2,j} - w_{i-2,j}\right) + \frac{1}{60}\left(w_{i+3,j} - w_{i-3,j}\right)\right) + O\left(h^6\right), i = \overline{3, n_2 - 3}, j = \overline{1, n_1 - 1}, \\ w_{y(1,j)} = \frac{1}{h}\left(-\frac{w_{0,j}}{5} - \frac{13}{12}w_{1,j} + 2w_{2,j} - w_{3,j} + \frac{w_{4,j}}{3} - \frac{w_{5,j}}{20}\right) + O\left(h^4\right), j = \overline{1, n_1 - 1}, \\ w_{y(2,j)} = \frac{1}{12h}\left(8\left(w_{3,j} - w_{1,j}\right) - \left(w_{4,j} - w_{0,j}\right)\right) + O\left(h^4\right), j = \overline{1, n_1 - 1}, \\ w_{y(n_2-1,j)} = -\frac{1}{h}\left(-\frac{w_{n_2,j}}{5} - \frac{13}{12}w_{n_2-1,j} + 2w_{n_2-2,j} - w_{n_2-3,j} + \frac{w_{n_2-4,j}}{3} - \frac{w_{n_2-5,j}}{20}\right) + O\left(h^4\right), j = \overline{1, n_1 - 1}, \\ w_{y(n_2-2,j)} = -\frac{1}{12h}\left(8\left(w_{n_2-3,j} - w_{n_2-1,j}\right) - \left(w_{n_2-4,j} - w_{n_2,j}\right)\right) + O\left(h^4\right), j = \overline{1, n_1 - 1}. \end{cases} \tag{7}$$

The second-order partial derivatives w_{yy} in (6) are expressed as follows:

$$\begin{cases} w_{yy(i,j)} = \frac{1}{h^2}\left(-\frac{49}{18}w_{i,j} + \frac{3}{2}\left(w_{i+1,j} + w_{i-1,j}\right) - \frac{3}{20}\left(w_{i+2,j} + w_{i-2,j}\right) + \frac{1}{90}\left(w_{i+3,j} + w_{i-3,j}\right)\right) + O\left(h^6\right), i = \overline{3, n_2 - 3}, j = \overline{1, n_1 - 1}, \\ w_{yy(1,j)} = \frac{1}{h^2}\left(\frac{137}{180}w_{0,j} - \frac{49}{60}w_{1,j} - \frac{17}{12}w_{2,j} + \frac{47}{18}w_{3,j} - \frac{19}{12}w_{4,j} + \frac{31}{60}w_{5,j} - \frac{13}{180}w_{6,j}\right) + O\left(h^4\right), j = \overline{1, n_1 - 1}, \\ w_{yy(2,j)} = \frac{1}{h^2}\left(-\frac{5}{2}w_{2,j} + \frac{4}{3}\left(w_{1,j} + w_{3,j}\right) - \frac{1}{12}\left(w_{0,j} + w_{4,j}\right)\right) + O\left(h^4\right), j = \overline{1, n_1 - 1}, \\ w_{yy(n_2-1,j)} = \frac{1}{h^2}\left(\frac{137}{180}w_{n_2,j} - \frac{49}{60}w_{n_2-1,j} - \frac{17}{12}w_{n_2-2,j} + \frac{47}{18}w_{n_2-3,j} - \frac{19}{12}w_{n_2-4,j} + \frac{31}{60}w_{n_2-5,j} - \frac{13}{180}w_{n_2-6,j}\right) + O\left(h^4\right), j = \overline{1, n_1 - 1}, \\ w_{yy(n_2-2,j)} = \frac{1}{h^2}\left(-\frac{5}{2}w_{n_2-2,j} + \frac{4}{3}\left(w_{n_2-1,j} + w_{n_2-3,j}\right) - \frac{1}{12}\left(w_{n_2,j} + w_{n_2-4,j}\right)\right) + O\left(h^4\right), j = \overline{1, n_1 - 1}. \end{cases} \tag{8}$$

Similarly, the formulas for the derivative w_{xx} are written analogously to formulas (8). From [2], we also include the general boundary condition for vorticity (equation (6), sixth step of the general algorithm) in the open cavity with fourth-order accuracy, obtained by differentiating the last equation for the stream function in system (1) twice with respect to y:

$$w(x,y) = -\psi_{xx} - \psi_{yy} = \frac{1}{h_1^2}\left(\frac{415}{72}\psi_0 - 8\psi_1 + 3\psi_2 - \frac{8}{9}\psi_3 + \frac{1}{8}\psi_4\right) - \frac{25}{6}\frac{v(0,y)}{h_1} - \psi_{yy}, v = -\psi_x,$$
$$m = \overline{0, n_2}, y_m = mh_2, \Delta = h_2\left(n_2 - n_3\right), 1 - \Delta = h_2 n_3, \tag{9}$$

$$\overline{w}_{m,0} = \begin{cases} \frac{1}{h_1^2}\left(\frac{415}{72}\overline{\psi}_{m,0} - 8\overline{\psi}_{m,1} + 3\overline{\psi}_{m,2} - \frac{8}{9}\overline{\psi}_{m,3} + \frac{1}{8}\overline{\psi}_{m,4}\right) - \frac{25}{6}\frac{\overline{v}_{m,0}}{h_1} + 2\frac{\left(\overline{y_m} - H/L\right)}{\left(\Delta/L\right)^2}, m = \overline{n_3, n_2}, \\ \frac{1}{h_1^2}\left(\frac{415}{72}\overline{\psi}_{m,0} - 8\overline{\psi}_{m,1} + 3\overline{\psi}_{m,2} - \frac{8}{9}\overline{\psi}_{m,3} + \frac{1}{8}\overline{\psi}_{m,4}\right) - \frac{25}{6}\frac{\overline{v}_{m,0}}{h_1}, m = \overline{0, n_3}, \textit{left}, \end{cases} \tag{10.1}$$

$$\overline{w}_{m,n_1} = \begin{cases} \frac{1}{h_1^2}\left(\frac{415}{72}\overline{\psi}_{m,n_1} - 8\overline{\psi}_{m,n_1-1} + 3\overline{\psi}_{m,n_1-2} - \frac{8}{9}\overline{\psi}_{m,n_1-3} + \frac{1}{8}\overline{\psi}_{m,n_1-4}\right) + \frac{25}{6}\frac{\overline{v}_{m,n_1}}{h_1} + 2\frac{\left(\overline{y_m} - H/L\right)}{\left(\Delta/L\right)^2}, m = \overline{n_3, n_2}, \\ \frac{1}{h_1^2}\left(\frac{415}{72}\overline{\psi}_{m,n_1} - 8\overline{\psi}_{m,n_1-1} + 3\overline{\psi}_{m,n_1-2} - \frac{8}{9}\overline{\psi}_{m,n_1-3} + \frac{1}{8}\overline{\psi}_{m,n_1-4}\right) + \frac{25}{6}\frac{\overline{v}_{m,n_1}}{h_1}, m = \overline{0, n_3}, \quad \textit{right}, \end{cases} \tag{10.2}$$

$$\overline{w}_{0,n}=\begin{cases}\dfrac{1}{h_2^2}\left(\dfrac{415}{72}\overline{\psi}_{0,n}-8\overline{\psi}_{1,n}+3\overline{\psi}_{2,n}-\dfrac{8}{9}\overline{\psi}_{3,n}+\dfrac{1}{8}\overline{\psi}_{4,n}\right)+\dfrac{25}{6}\dfrac{\overline{u}_{0,n}}{h_2},\ n=\overline{0,n_1},\ u=\psi_y,\ bottom,\\ \dfrac{1}{h_2^2}\left(\dfrac{415}{72}\overline{\psi}_{n_2,n}-8\overline{\psi}_{n_2-1,n}+3\overline{\psi}_{n_2-2,n}-\dfrac{8}{9}\overline{\psi}_{n_2-3,n}+\dfrac{1}{8}\overline{\psi}_{n_2-4,n}\right)-\dfrac{25}{6}\dfrac{\overline{u}_{n_2,n}}{h_2},\ n=\overline{0,n_1},\ top.\end{cases} \tag{10.3}$$

In deriving the boundary equation (9) for the vorticity function, all stream function derivatives of order higher than two were eliminated. This significantly improves the stability of boundary finite-difference conditions of the type (9) and (10) for velocity fields with first-kind discontinuities. Table 1 presents the classification of blood vessels according to their Reynolds number and diameter.

Table 1

Classification of blood vessels

Type	Diameter	Blood velocity	Re	Governing equations
Capillaries	(5–10) μm	(0.5–1.0) mm/s	0.00075–0.003	–
Arterioles	(10–100) μm	(0.5–10.0) cm/s	0.015–3,000	(1), (13)
Arteries	(2–10) mm	(10.0–50.0) cm/m	60–1500	(1), (13)
Aorta	(2–3) cm	0.5 m/s	3000	(1), (13)

Experience [1] shows that, for a physically rapid solution of system (1) in arterioles and arteries, it is necessary to select an inertial time interval $T=\dfrac{L}{u_{\max}}$, while the hydrodynamic problem is solved using system (1).

We consider a simplest mathematical model of fibrin formation, which accounts for the concentration dynamics of two metabolites: an activator of the coagulation process (thrombin) s and an inhibitor z, which slows down blood coagulation:

$$\begin{cases}\dfrac{\partial s}{\partial t}+u\dfrac{\partial s}{\partial x}+v\dfrac{\partial s}{\partial y}=D\left(s_{xx}+s_{yy}\right)+\dfrac{\alpha s^2}{s+s_0}-k_1 s-\gamma s z,\\ \dfrac{\partial z}{\partial t}+u\dfrac{\partial z}{\partial x}+v\dfrac{\partial z}{\partial y}=D\left(z_{xx}+z_{yy}\right)+\beta s\left(1-\dfrac{z}{c}\right)\left(1+\dfrac{z^2}{z_0^2}\right)-k_2 z.\end{cases} \tag{11}$$

Here, u, v are the velocity components; the coefficients α, β, k_1, γ, D, c, v_0, k_2 are dimensional, and their numerical values are taken from [3, p. 16].

Table 2

Dimensional coefficients in system of equations (11)

α, min^{-1}	β, min^{-1}	$\dfrac{\gamma}{\min\cdot\mathrm{nM}}$	$v_0(z_0)$, nM	c, nM	$u_0(s_0)$, nM	k_1, min^{-1}	k_2, min^{-1}
2.0	0.0015	5.0	0.0525	5.0	2.95	0.05	0.35

The diffusion coefficients of thrombin and the inhibitor are assumed equal to $D = 10^{-11}$ m^2/s [2, p. 99]. The diffusion velocities of thrombin and the inhibitor can be calculated using the formula $v=2\sqrt{\alpha D}=2\sqrt{10^{-11}2/60}=1.155\cdot10^{-6}$ m/s. These diffusion velocities are significantly smaller than the blood velocity in an arteriole (3 mm/s) and in an artery (50 cm/s), which justifies the inclusion of advection terms on the left-hand side of system (11).

$$\begin{cases}\dfrac{\partial\overline{s}}{T\partial\overline{t}}+\dfrac{u_{\max}}{L}\overline{u}\dfrac{\partial\overline{s}}{\partial\overline{x}}+\dfrac{u_{\max}}{L}\overline{v}\dfrac{\partial\overline{s}}{\partial\overline{y}}=\dfrac{D}{L^2}\left(\overline{s}_{\overline{x}\overline{x}}+\overline{s}_{\overline{y}\overline{y}}\right)+\dfrac{\alpha\overline{s}^2}{\overline{s}+1}-k_1\overline{s}-\gamma\overline{s}\overline{z}z_0,\\ \dfrac{\partial\overline{z}}{T\partial\overline{t}}+\dfrac{u_{\max}}{L}\overline{u}\dfrac{\partial\overline{z}}{\partial\overline{x}}+\dfrac{u_{\max}}{L}\overline{v}\dfrac{\partial\overline{z}}{\partial\overline{y}}=\dfrac{D}{L^2}\left(\overline{z}_{\overline{x}\overline{x}}+\overline{z}_{\overline{y}\overline{y}}\right)+\dfrac{s_0}{z_0}\beta\overline{s}\left(1-\dfrac{z_0\overline{z}}{c}\right)\left(1+\overline{z}^2\right)-k_2\overline{z},\end{cases}\Leftrightarrow$$

$$\begin{cases}\dfrac{\partial\overline{s}}{\partial\overline{t}}+\overline{u}\dfrac{\partial\overline{s}}{\partial\overline{x}}+\overline{v}\dfrac{\partial\overline{s}}{\partial\overline{y}}=\dfrac{D}{Lu_{\max}}\left(\overline{s}_{\overline{x}\overline{x}}+\overline{s}_{\overline{y}\overline{y}}\right)+\dfrac{L}{u_{\max}}\left(\dfrac{\alpha\overline{s}^2}{\overline{s}+1}-k_1\overline{s}-\gamma\overline{s}\overline{z}z_0\right),\\ \dfrac{\partial\overline{z}}{\partial\overline{t}}+\overline{u}\dfrac{\partial\overline{z}}{\partial\overline{x}}+\overline{v}\dfrac{\partial\overline{z}}{\partial\overline{y}}=\dfrac{D}{Lu_{\max}}\left(\overline{z}_{\overline{x}\overline{x}}+\overline{z}_{\overline{y}\overline{y}}\right)+\dfrac{L}{u_{\max}}\left(\dfrac{s_0}{z_0}\beta\overline{s}\left(1-\dfrac{z_0\overline{z}}{c}\right)\left(1+\overline{z}^2\right)-k_2\overline{z}\right),\end{cases}\Leftrightarrow$$

$$\begin{cases} \dfrac{\partial \bar{s}}{\partial \bar{t}} + \bar{u}\dfrac{\partial \bar{s}}{\partial \bar{x}} + \bar{v}\dfrac{\partial \bar{s}}{\partial \bar{y}} = \dfrac{D}{\nu \mathrm{Re}}\left(\bar{s}_{\bar{x}\bar{x}} + \bar{s}_{\bar{y}\bar{y}}\right) + \dfrac{L}{u_{\max}}\left(\dfrac{\alpha \bar{s}^2}{\bar{s}+1} - k_1 \bar{s} - \gamma \bar{s}\bar{z}z_0\right), \\ \dfrac{\partial \bar{z}}{\partial \bar{t}} + \bar{u}\dfrac{\partial \bar{z}}{\partial \bar{x}} + \bar{v}\dfrac{\partial \bar{z}}{\partial \bar{y}} = \dfrac{D}{\nu \mathrm{Re}}\left(\bar{z}_{\bar{x}\bar{x}} + \bar{z}_{\bar{y}\bar{y}}\right) + \dfrac{L}{u_{\max}}\left(\dfrac{s_0}{z_0}\beta \bar{s}\left(1 - \dfrac{z_0 \bar{z}}{c}\right)\left(1 + \bar{z}^2\right) - k_2 \bar{z}\right), \\ \dfrac{d\bar{\varphi}}{d\bar{t}} = \bar{s}(\bar{t}). \end{cases} \tag{12}$$

The last equation in system (12) is the thrombin growth equation $\bar{\varphi}(\bar{t})$ obtained by integrating the activator $\bar{s}(\bar{t})$ over the dimensionless time $\bar{t}$. According to [2–5], the activator $\bar{s}(\bar{t})$, the inhibitor $\bar{z}(\bar{t})$, and thrombin $\bar{\varphi}(\bar{t})$ take only non-negative values, which was enforced by the authors in the numerical implementation.

For an arteriole [5], the diameter is $2d = 2$ mm, the blood viscosity is $\eta = 3{,}5 \cdot 10^{-3}$ Pa·s, and the kinematic viscosity of blood is $\nu = \dfrac{\mu}{\rho} = \dfrac{3.5 \cdot 10^{-3}\,\mathrm{Pa \cdot s}}{1050\ \mathrm{kg/m^3}} = 3.33(3) \cdot 10^{-6}\,\dfrac{\mathrm{m}^2}{\mathrm{s}}$. The blood velocity [5] in an aneurysm of diameter $L \approx 4d = 4$ mm is $u_{\max} = 3$ mm/s. Then the Reynolds number is calculated as $\mathrm{Re} = \dfrac{u_{\max} L}{\nu} = \dfrac{3 \cdot 10^{-3} \cdot 4 \cdot 10^{-3}}{3.33(3) \cdot 10^{-6}} = 3.6$. We introduce the following dimensionless variables $\bar{s} = s / s_0$, $\bar{z} = z / z_0$, and compute the corresponding dimensionless coefficients:

$$\frac{D}{\nu \mathrm{Re}} = \frac{10^{-11}}{3.33(3) \cdot 10^{-6} \cdot 3.6} = 8.33(3) \cdot 10^{-7},\ z_0 / C = 0.0525/5 = 1.05 \cdot 10^{-2},\ z_0 / C = 0.0525/5 = 1.05 \cdot 10^{-2},$$

$$\alpha \frac{L}{u_{\max}} = \frac{2 \cdot 4 \cdot 10^{-3}}{60 \cdot 3 \cdot 10^{-3}} = 0.044(4),\ k_1 \frac{L}{u_{\max}} = \frac{0.05 \cdot 4 \cdot 10^{-3}}{60 \cdot 3 \cdot 10^{-3}} = 0.0011(1),$$

$$\frac{L\gamma}{u_{\max}} z_0 = \frac{4 \cdot 10^{-3}}{3 \cdot 10^{-3}} \cdot \frac{5}{60} \cdot 0.0525 = 0.005833(3),\ k_2 \frac{L}{u_{\max}} = \frac{0.35 \cdot 4 \cdot 10^{-3}}{60 \cdot 3 \cdot 10^{-3}} = 0.0077(7),$$

$$\frac{L\beta}{u_{\max}} \frac{s_0}{z_0} = \frac{4 \cdot 10^{-3}}{3 \cdot 10^{-3}} \cdot \frac{0.0015}{60} \cdot \frac{2.95}{0.0525} = 0.00187301587301(587301).$$

We denote the right-hand sides in the dynamical equations for the inhibitor and activator in system (12) and obtain the splitting method [11] with splitting multiplicity N:

$$F_{\bar{s}}\left(\bar{t} = \tau_0\left(k + (i/N)\right), \bar{x}, \bar{y}\right) = \frac{D}{\nu \mathrm{Re}}\left(\bar{s}_{\bar{x}\bar{x}} + \bar{s}_{\bar{y}\bar{y}}\right) + \frac{L}{u_{\max}}\left(\frac{\alpha \bar{s}^2}{\bar{s}+1} - k_1 \bar{s} - \gamma \bar{s}\bar{z}z_0\right),$$

$$F_{\bar{z}}\left(\bar{t} = \tau_0\left(k + (i/N)\right), \bar{x}, \bar{y}\right) = \frac{D}{\nu \mathrm{Re}}\left(\bar{z}_{\bar{x}\bar{x}} + \bar{z}_{\bar{y}\bar{y}}\right) + \frac{L}{u_{\max}}\left(\frac{s_0}{z_0}\beta \bar{s}\left(1 - \frac{z_0 \bar{z}}{c}\right)\left(1 + \bar{z}^2\right) - k_2 \bar{z}\right),$$

$$\begin{cases} \dfrac{\bar{s}^{k+((i+1)/N)} - \bar{s}^{k+(i/N)}}{\tau_0 / N} + u^k \cdot \bar{s}_x^{k+(i/N)} + v^k \cdot \bar{s}_y^{k+(i/N)} = F_{\bar{s}}\left(\bar{t} = \tau_0\left(k + (i/N)\right), \bar{x}, \bar{y}\right), \\ \dfrac{\bar{z}^{k+((i+1)/N)} - \bar{z}^{k+(i/N)}}{\tau_0 / N} + u^k \cdot \bar{z}_x^{k+(i/N)} + v^k \cdot \bar{z}_y^{k+(i/N)} = F_{\bar{z}}\left(\bar{t} = \tau_0\left(k + (i/N)\right), \bar{x}, \bar{y}\right), i = \overline{0, N-1},\ k = 0,1,2,\ldots. \end{cases} \tag{13}$$

The splitting multiplicity $N = 70$ in system (13) for the inhibitor and activator differs from the multiplicity $n = 200$ used for the vorticity equation (6). It is only necessary to synchronize the time steps of systems (6) and (13) such that, after completion of both subroutine loops, the increment of their dimensionless time coincides, i. e., equals τ_0.

If the boundary conditions for the inhibitor and activator at the solid wall are specified for the no-penetration case (for example, at the bottom of the cavity), then from formula (5.1) we obtain formula (14.1) with eleventh-order accuracy:

$$\begin{aligned} 0 = \bar{s}_y(0, j) = \frac{1}{(-h_2)}\Bigg(& -\frac{83711}{27720}\bar{s}_{0,j} + 11\bar{s}_{1,j} - \frac{55}{2}\bar{s}_{2,j} + 55\bar{s}_{3,j} - \frac{165}{2}\bar{s}_{4,j} + \frac{462}{5}\bar{s}_{5,j} - \\ & -77\bar{s}_{6,j} + \frac{330}{7}\bar{s}_{7,j} - \frac{165}{8}\bar{s}_{8,j} + \frac{55}{9}\bar{s}_{9,j} - \frac{11}{10}\bar{s}_{10,j} + \frac{1}{11}\bar{s}_{11,j}\Bigg) + O\left(h^{10}\right), j = \overline{1, n_1 - 1} \Leftrightarrow \\ \bar{s}_{0,j} = \frac{27720}{83711}\Bigg(& 11\bar{s}_{1,j} - \frac{55}{2}\bar{s}_{2,j} + 55\bar{s}_{3,j} - \frac{165}{2}\bar{s}_{4,j} + \frac{462}{5}\bar{s}_{5,j} - \end{aligned} \tag{14.1}$$

$$-77\bar{s}_{6,j}+\frac{330}{7}\bar{s}_{7,j}-\frac{165}{8}\bar{s}_{8,j}+\frac{55}{9}\bar{s}_{9,j}-\frac{11}{10}\bar{s}_{10,j}+\frac{1}{11}\bar{s}_{11,j}\Big)+O\left(h^{11}\right),\ j=\overline{1,n_1-1}.$$

Similarly, we obtain formula (14.2) with fifth-order accuracy:

$$\bar{s}_{0,j}=\frac{60}{137}\left(5\bar{s}_{1,j}-5\bar{s}_{2,j}+\frac{10}{3}\bar{s}_{3,j}-\frac{5}{4}\bar{s}_{4,j}+\frac{1}{5}\bar{s}_{5,j}\right)+O\left(h^5\right),\ j=\overline{1,n_1-1}. \tag{14.2}$$

Problem Initialization. The initial values for the inhibitor and activator fields are set, following A.I. Lobanov [3], as a step function for the activator. These initial conditions were used in systems (1) and (13), with the solutions shown below in Fig. 2–7:

$$\begin{cases}\bar{z}_{i,j}(t=0)=0,\forall i=\overline{0,n_2},\ j=\overline{0,n_1},\\ \bar{s}_{i,j}(t=0)=\begin{cases}1,\forall i=\overline{0,n_2},\ j=\overline{0,n_1/2},\\ 0,\forall i=\overline{0,n_2},\ j=\overline{n_1/2,n_1}.\end{cases}\end{cases} \tag{15}$$

We also assume that the boundary conditions for the activator and inhibitor on the rectangular boundary of the cavity (aneurysm) are homogeneous. Dirichlet conditions:

$$\bar{s}\big|_{\Gamma/\Gamma_2}=0,\bar{z}\big|_{\Gamma/\Gamma_2}=0. \tag{16}$$

The initial velocity field is defined as follows: the vertical velocity component $v_{i,j}(t=0)$ is absent, while the horizontal component $u_{i,j}(t=0)$ follows a Poiseuille distribution (4):

$$\begin{cases}v_{i,j}(t=0)=0,\forall i=\overline{0,n_2},\ j=\overline{0,n_1},\\ u_{i,j}(t=0)=\begin{cases}\left(1-\left(\dfrac{\overline{y_i}-\overline{H}}{\overline{\Delta}}\right)^2\right),\ \overline{H}-\overline{\Delta}=h_2n_3\le\overline{y_i}\le\overline{H}=h_2n_2,\overline{y_i}=i\cdot h_2,i=\overline{n_3,n_2},\\ 0,i=\overline{0,n_3}.\end{cases}\end{cases} \tag{17}$$

From [5], we select an arteriole diameter of $2d=2$ mm and a blood velocity $u=3$ mm/s. The aneurysm diameter and length are twice that, $2D=L=4$ мм. The corresponding Reynolds number is $\mathrm{Re}=\dfrac{u_{\max}L}{\nu}=\dfrac{3\cdot10^{-3}\cdot4\cdot10^{-3}}{3.333\cdot10^{-6}}=3.6$. The **transit time** of a fluid particle $T=\dfrac{L}{u_{\max}}=\dfrac{4\cdot10^{-3}}{3\cdot10^{-3}}=1.33(3)$ s along the aneurysm exceeds the period of cardiac pulsations (1 second); therefore, during the time interval $T=1.33(3)$ s two cardiac pulsations occur, resulting in two mechanical mixing events of the blood within the aneurysm walls.

Homogeneous zero boundary conditions were chosen for the inhibitor and activator on the cavity walls, based on the assumption that their concentrations at points far from the aneurysm are zero. On the upper segment of the cavity, formula (14.2) was applied for both the activator and inhibitor, as symmetric solutions are sought for all unknown fields. System (12) has a trivial solution $\bar{s}(\bar{t})=\bar{z}(\bar{t})\equiv0$. As shown in [3], the trivial solutions $\bar{s}(\bar{t})=\bar{z}(\bar{t})\equiv0$ are stable if the inhibitor and activator values remain below their threshold levels $\bar{s}(\bar{t})=\bar{z}(\bar{t})\equiv0$. This justifies the use of homogeneous zero boundary conditions.

The initial fibrin field $\varphi(\bar{t})$ in (12), obtained by integrating the activator field over time, at $T=1.33(3)$ *s* is shown in Fig. 2.

From Fig. 2, it follows that even at the initial stage of fibrin formation, noticeable transport occurs — both advection along the blood flow and diffusion, according to system (13).

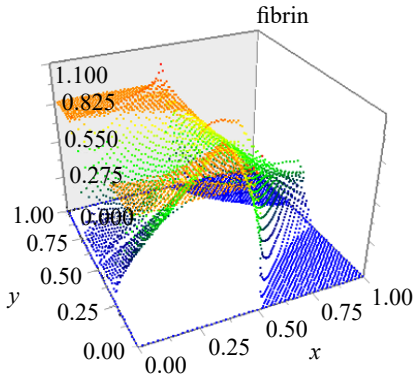

a)

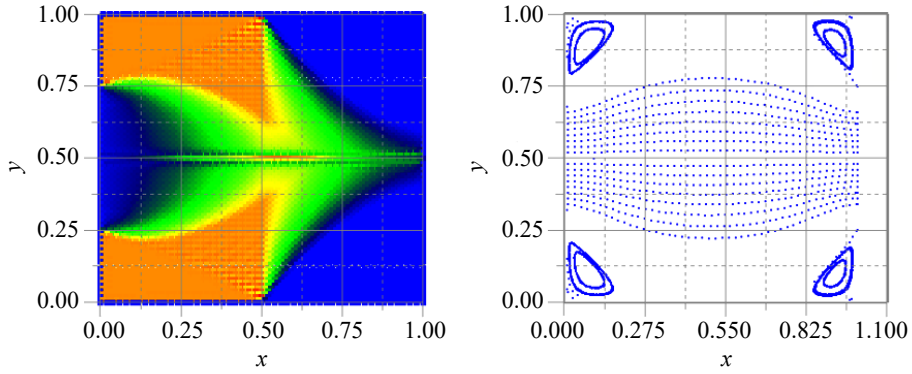

Fig. 2. Fields in an arteriole using formula (14.2) at $T = 1.33(3)$ s,
Re = 3.6, $n_1 \times n_2 = 100 \times 50$, $\Delta / H = 0.5$; $L = 4$ mm, $2H = 4$ mm, $u_{\max} = 3$ mm/s, $\tau = \frac{6}{16} h_1^2$, $m = 53000$ steps,
splitting multiplicities $n = 200$ in (6), $N = 70$ in (13):
a — fibrin surface; *b* — fibrin distribution in the aneurysm; *c* — streamlines in the aneurysm

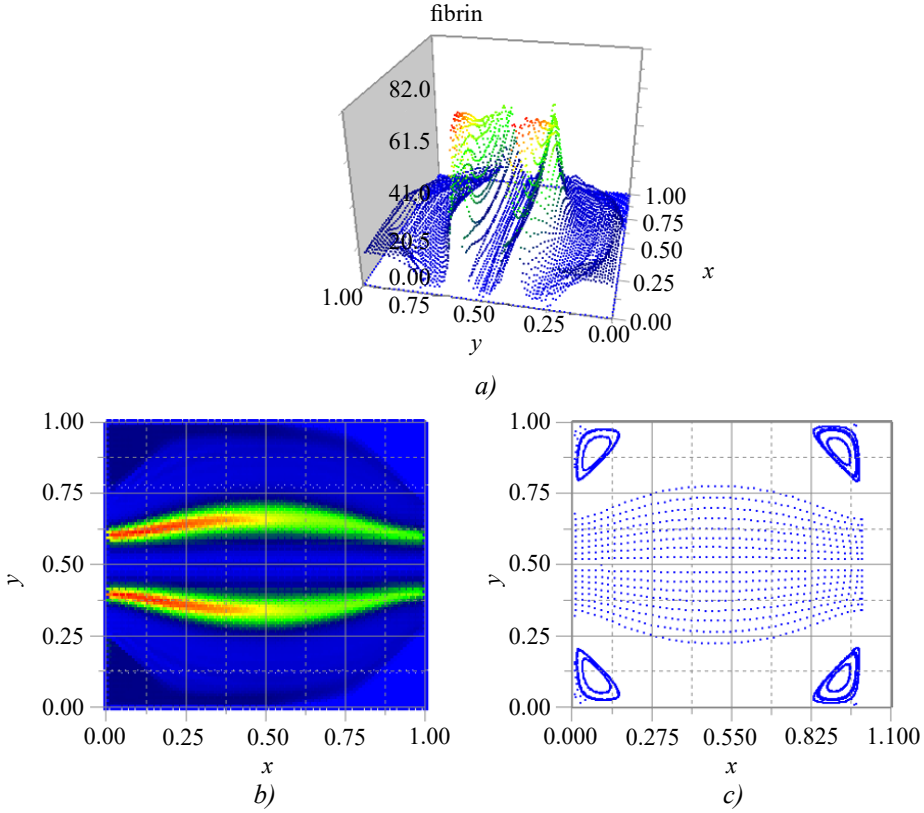

Fig. 3. Fields in an arteriole using formula (14.2) at $T = 20$ s,
Re = 3.6, $n_1 \times n_2 = 100 \times 50$, $\Delta / H = 0.5$; $L = 4$ mm, $2H = 4$ mm, $u_{\max} = 3$ mm/s, $\tau = \frac{6}{16} h_1^2$, $m = 800000$ steps,
splitting multiplicities $n = 200$ in (6), $N = 70$ in (13):
a — fibrin surface; *b* — fibrin distribution in the aneurysm; *c* — streamlines in the aneurysm

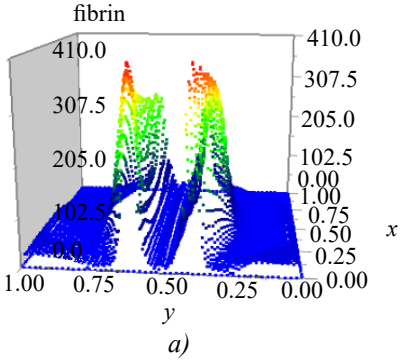

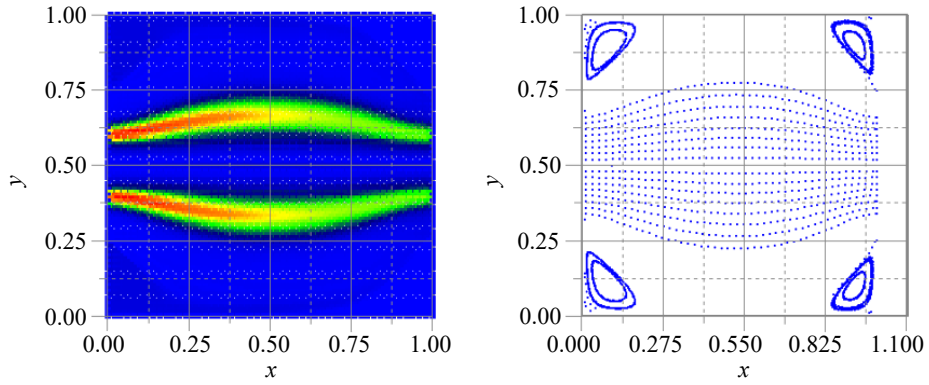

Fig. 4. Fields in an arteriole using formula (14.2) at $T = 26$ s,
$\mathrm{Re} = 3.6$, $n_1 \times n_2 = 100 \times 50$, $\Delta / H = 0.5$; $L = 4$ mm, $2H = 4$ mm, $u_{\max} = 3$ mm/s, $\tau = \frac{6}{16} h_1^2$, $m = 1200000$ steps,
splitting multiplicities $n = 200$ in (6), $N = 70$ in (13):
a — fibrin surface; *b* — fibrin distribution in the aneurysm; *c* — streamlines in the aneurysm

Fig. 4 concludes the graphical representation of thrombus formation in an arteriole aneurysm at the end of the first phase (30 seconds). From Table 1, we select an artery diameter of $2d = 1$ cm and a blood velocity $u = 0.5$ m/s. The aneurysm diameter and length are twice that, $2H = L = 2$ cm. The corresponding Reynolds number is $\mathrm{Re} = \frac{u_{\max} L}{\nu} = \frac{0.5 \cdot 2 \cdot 10^{-2}}{3.33(3) \cdot 10^{-6}} = 3000$. The transit time of a fluid particle $T = \frac{L}{u_{\max}} = \frac{2 \cdot 10^{-2}}{0.5} = 0.04$ s along the aneurysm is less than the period of cardiac pulsations (1 second); therefore, during this interval $T = 0.04$ s only a single cardiac pulsation occurs, resulting in blood mixing within the aneurysm with low probability.

The initial fibrin field $\bar{\varphi}(\bar{t})$ in (12), obtained by integrating the activator field over time, at $T = 0.04$ s is shown in Fig. 5.

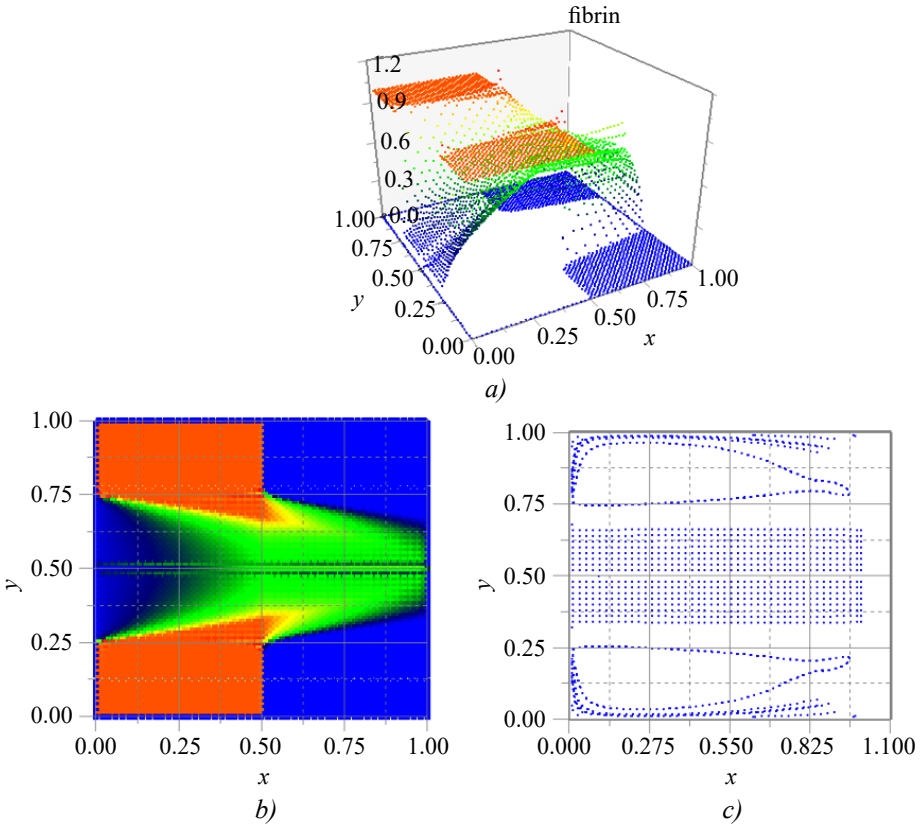

Fig. 5. Fields in an artery using formula (14.2) at $T = 0.04$ s,
$\mathrm{Re} = 3000$, $n_1 \times n_2 = 100 \times 50$, $\Delta / H = 0.5$; $L = 2$ cm, $2H = 2$ cm, $u_{\max} = 0.5$ m/s, $\tau = \frac{6}{16} h_1^2$, $m = 53000$ steps,
splitting multiplicities $n = 200$ in (6), $N = 70$ in (13):
a — fibrin surface; *b* — fibrin distribution in the aneurysm; *c* — streamlines in the aneurysm

Compared to Fig. 2*b*, in Fig. 5*b* the advection of the activator is more pronounced than its diffusion. In Fig. 6*b*, the fibrin transport along the flow and its swirling near the right segment of the cavity, forming a “fibrin stalk”, can be observed. Consequently, a fibrin film forms along the geometric boundary of the cavity, blocking oxygen access to the aneurysm walls and creating blood stasis within the aneurysm.

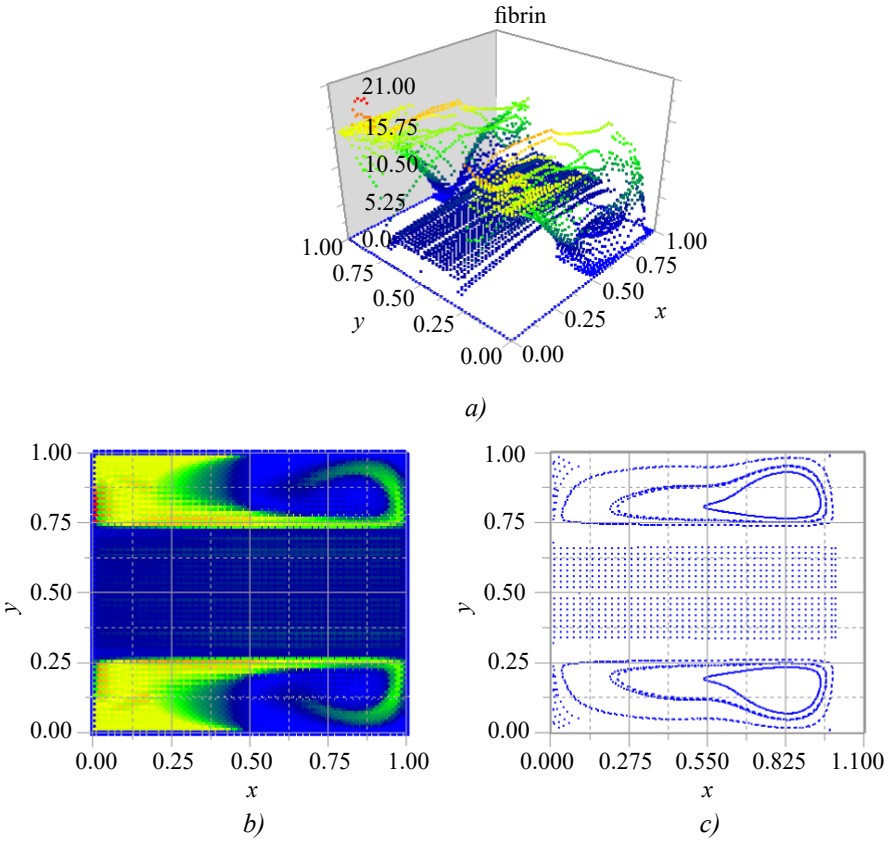

Fig. 6. Fields in an artery using formula (14.2) at $T = 0.6$ s,
$\mathrm{Re} = 3000$, $n_1 \times n_2 = 100 \times 50$, $\Delta / H = 0.5$; $L = 2$ cm, $2H = 2$ cm, $u_{\max} = 0.5$ m/s, $\tau = \frac{6}{16} h_1^2$, $m = 800000$ steps,
splitting multiplicities $n = 200$ in (6), $N = 70$ in (13):
a — fibrin surface; *b* — fibrin distribution in the aneurysm; *c* — streamlines in the aneurysm

Qualitatively, Fig. 6 and 7 are similar; however, the “fibrin stalk” in Fig. 6*b* has already transformed into a “fibrin ring” in Fig. 7*b*. Fig. 6 and 7 demonstrate that in a turbulent environment, each fibrin filament rapidly changes its value even along its length, resembling loose hair strands blown by the wind.

Next, we consider the periodic structure of fibrin in an arteriole near the aneurysm wall at $t = 10$ s after the onset of blood coagulation, as shown in Fig. 8.

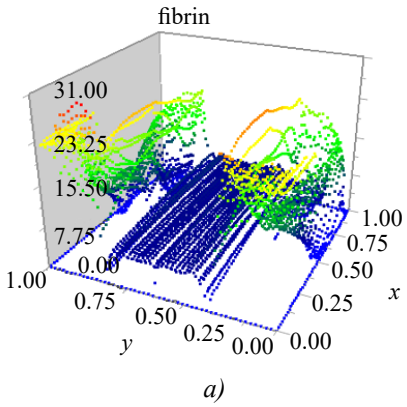

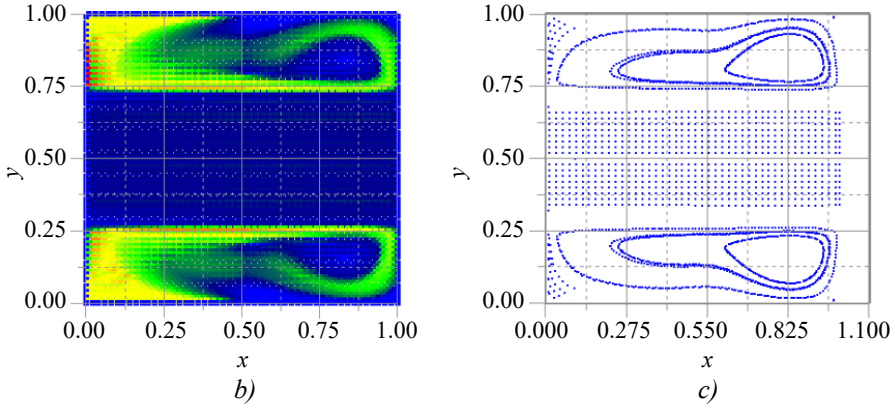

Fig. 7. Fields in an artery using formula (14.2) at $T = 0.9$ s,
$\mathrm{Re} = 3000$, $n_1 \times n_2 = 100 \times 50$, $\Delta / H = 0.5$; $L = 2$ cm, $2H = 2$ cm, $u_{\max} = 0.5$ m/s, $\tau = \frac{6}{16} h_1^2$, $m = 1200000$ steps,
splitting multiplicities $n = 200$ in (1), $N = 70$ in (13):
a — fibrin surface; *b* — fibrin distribution in the aneurysm; *c* — streamlines in the aneurysm

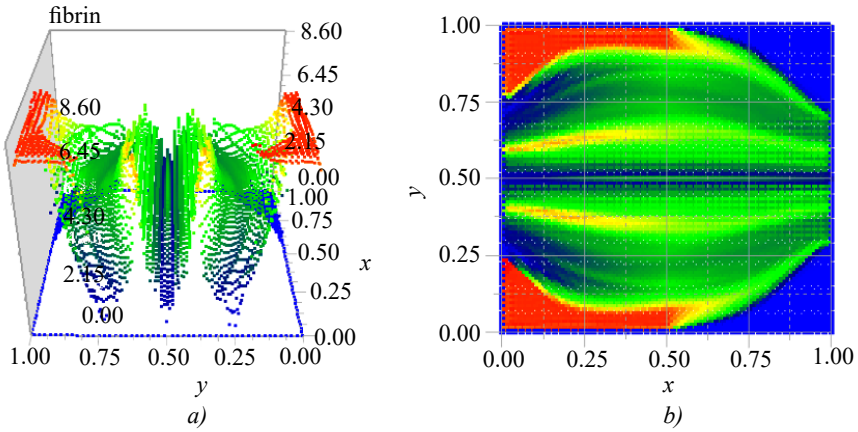

Fig. 8. Fibrin field in an arteriole using formula (14.2) at $T = 10$ s,
$\mathrm{Re} = 3.8$, $n_1 \times n_2 = 100 \times 50$, $\Delta / H = 0.5$; $L = 4$ mm, $2H = 4$ mm, $u_{\max} = 3$ mm/s, $\tau = \frac{6}{16} h_1^2$, $m = 400000$ steps,
splitting multiplicities $n = 200$ in (6), $N = 70$ in (13):
a — fibrin surface; *b* — fibrin distribution in the aneurysm

Fig. 8*a* and 8*b* show that fibrin moves along the aneurysm wall in a thin layer against the direction of blood flow (at a velocity of $u_{\max} = 3$ mm/s). It turns at the far wall (potentially adhering to it) and returns to the near wall, forming a "fibrin horseshoe" with the maximum fibrin density located outside the aneurysm region. That is, the fibrin horseshoe grows both within the bulk of the flow and against the flow direction. In Fig. 8*b*, a periodic spatial variation of fibrin density along the aneurysm wall is also visible. Similarly, in Fig. 3*b* and 4*b*, the fibrin horseshoe in the center of the arteriole aneurysm reaches its maximum density (shown in red) near the left wall, confirming that fibrin growth occurs opposite to the direction of blood flow.

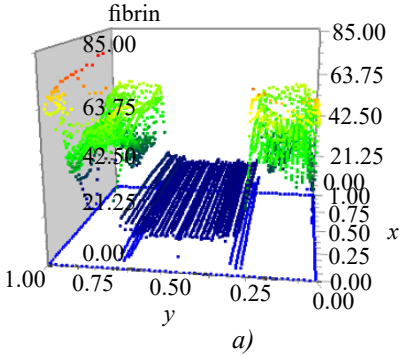

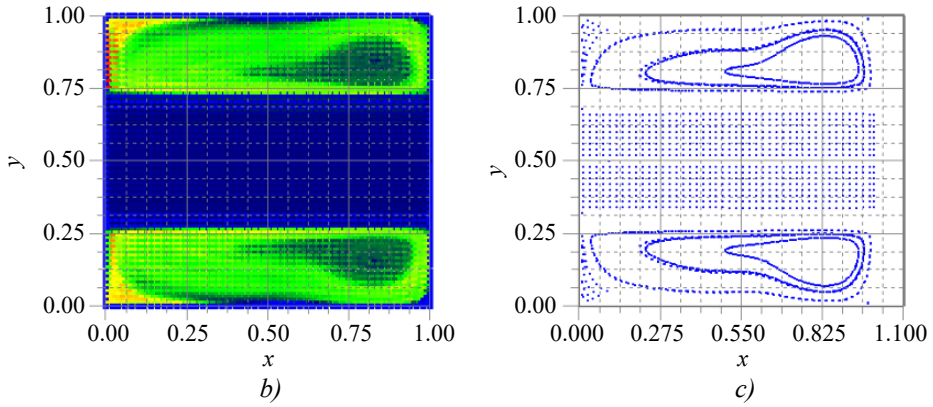

Fig. 9. Field distributions in the artery using (14.2) at $T = 2.54$ s

Re = 3000, $n_1 \times n_2 = 100 \times 50$, $\Delta / H = 0.5$; $L = 2\ cm, 2H = 2\ cm$, $u_{\max} = 0.5\ m/s$, $\tau = \frac{6}{16} h_1^2$, $m = 3387700$ steps,

splitting multiplicity $n = 200$ in (1), $N = 70$ in (13):

a — fibrin surface; *b* — fibrin distribution within the aneurysm; *c* — streamline field in the aneurysm

Fig. 9*b* shows that by $t = 2.54$ s, a homogeneous thrombus with a maximum dimensionless density of 85 units forms throughout the entire volume of the aneurysm (compared to Fig. 7*b*). The question of the threshold fibrin density is also crucial—the density at which it can be considered a solid body and impermeable to blood flow. In this case, blood must flow around the ultra-dense fibrin clots. It is equally important to obtain an experimental dependence of blood viscosity on the dimensionless fibrin density to account for it in the systems of equations (1) and (12).

Discussion

1. In the initial phase (Fig. 2*b* and 5*b*), fibrin forms in regions where the activator concentration exceeds the threshold and is transported to other parts of the aneurysm by advection and diffusion.

2. In arterioles, during the initial phase at $t = 1{,}333$ s (Fig. 2*a* and 2*b*), the maximum fibrin concentration (red tones) is observed near the aneurysm walls. However, at $t = 20$ s (Fig. 3*a* and 3*b*), a fibrin horseshoe appears, with maximum fibrin values in the central flow, approximately twice as high as near the wall.

3. In arteries with high blood velocity (Re = 3000) fibrin accumulates within the aneurysm, separating its boundaries from the blood flow by a “fibrin filament” (Fig. 6*b*).

4. Due to the nonlinear terms in systems (12) and (13), fibrin motion in arterioles (Re = 3.6) occurs against the flow (Fig. 3*b*), whereas in arteries (Re = 3000) it occurs in the direction of blood flow (Fig. 6*b*).

5. In Fig. 8*a* and 8*b*, near the aneurysm wall with low blood velocity, a spatial structure with periodic variations in fibrin density is observed. This result is consistent with [2–4], whose solutions can exhibit layered fibrin formation in stationary blood.

6. Fig. 3*b* and 6*b* show that even in the symmetry plane of the aneurysm, where fibrin density is minimal (blue tones), the value remains greater than zero. This indicates that the presence of an aneurysm causes blood densification and increased viscosity throughout the aneurysm, although solid fibrin does not form at every point.

7. The range of dimensionless fibrin in this study is of the same order as in [2–4], i. e., from 50 to 750 dimensionless units (in our examples, less than 500 dimensionless units).

8. Doubling the aneurysm diameter relative to the vessel diameter increases the Reynolds number (Re = 3000 in the artery) and, as seen in Fig. 6 and 7, generates a flow reversal point near the vortex core. Therefore, the presence of an aneurysm leads to velocity field discontinuities and an increase in vorticity in the vicinity of the flow reversal point.

Conclusion. This study presents the systems of equations (1), (12), and (13) with boundary and initial conditions (14), (15), (16), and (17), constituting a simplified unsteady model of blood flow and fibrin (thrombus) formation in aneurysms of blood vessels. The proposed model allows for a qualitative investigation of the mechanisms of thrombus formation in arterial and arteriolar aneurysms, as well as in components of medical devices.

References

1. Volosova N.K., Volosov K.A., Volosova A.K., Karlov M.I., Pastukhov D.F., Pastukhov Yu.F. Modelling circulation in the aneurysms of blood vessels. *Computation Mathematics and Information Technologies*. 2025;9(3):30–43. (In Russ.) https://doi.org/10.23947/2587-8999-2025-9-3-30-43

2. Ataulakhanov F.I., Guria G.T., Sorochkina A.Yu. Spatial aspects of the dynamics of blood coagulation. Phenomenological model. *Biophysics*. 1994;39(1):97−106. (In Russ.)

3. Lobanov A.I., Storozhilova T.K., Zarnitsyna V.I., Ataullakhanov F.I. Comparison of two mathematical models to describe the spatial dynamics of the blood coagulation process. *Mathematical modeling*. 2003;15(1):14−28. (In Russ.)

4. Volosov K.A., Vdovina E.K., Pugina L.V. Modeling of “pulsatile” modes of blood coagulation dynamics. *Math modeling*. 2014;26(12):14–32. (In Russ.)

5. Kalugina M.D., Limareva M.Yu., Lobanov A.I. Non-stacionary models of growth of platelet thrombus. *Russian Biomechanics Jornal.* 2024;26(4):179–188. (In Russ.) https://doi.org/10.15593/RZhBiomeh/2024.4.15

6. Petrov A.G. High-precision numerical schemes for solving plane boundary value problems for a polyharmonic equation and their application to problems of hydrodynamics. *Applied Mathematics and Mechanics*. 2023;87(3):343–368. (In Russ.) https://doi.org/10.31857/S0032823523030128

7. Sukhinov A.I., Kolgunova O.V., Girmai M.Z., Nakhom O.S. A two -dimensional hydrodynamic model of coastal systems, taking into account evaporation. *Computation Mathematics and Information Technologies*. 2023;7(4):9–21. (In Russ.) https://doi.org/10.23947/2587-8999-2023-7-4-9-21

8. Ershova T.Ya. Boundary value problem for a third-order differential equation with a strong boundary layer. *Bulletin of Moscow University. Episode 15: Computational mathematics and cybernetics*. 2020;1:30–39. (In Russ.) https://doi.org/10.3103/S0278641920010057

9. Sitnikova M.A., Skulsky O.I. Flow of momentary anisotropic fluid in thin layers. *Bulletin of Perm University. Mathematics. Mechanics. Informatics*. 2015;28(1):56–62. (In Russ.)

10. Sidoryakina V.V., Solomaha D.A. Symmetrized versions of the Seidel and upper relaxation methods for solving two-dimensional difference problems of elliptic. *Computational Mathematics and Information Technologies*. 2023;7(3):12–19. (In Russ.) https://doi.org/10.23947/2587-8999-2023-7-3-12-19

11. Volosova N.K., Volosov K.A., Volosova A.K., Karlov M.I., Pastuhov D.F., Pastuhov Yu.F. The *N*-fold distribution of the obvious variable scheme for the equalization of the vortex in the viscous incompatible fluid. *Bulletin of the Perm University. Mathematics. Mechanics. Informatics*. 2023; 63(4):12–21. (In Russ.) https://doi.org/10.17072/1993-0550-2023-4-12-21

12. Bahvalov N.S., Zhidkov N.P., Kobelkov G.M. *Numerical methods: a textbook for students of physics and mathematics specialties of higher educational institutions.* Binom. lab. Knowledge; 2011. 636 p. (In Russ.)

About the Authors:

Natalya K. Volosova, Post-graduate Student of Bauman Moscow State Technical University (2nd Baumanskaya St. 5–1, Moscow, 105005, Russian Federation), ORCID, navalosova@yandex.ru

Konstantin A. Volosov, Doctor of Physical and Mathematical Sciences, Professor of the Department of Applied Mathematics of the Russian University of Transport (Obraztsova St. 9–9, Moscow, GSP-4, 127994, Russian Federation), ORCID, SPIN-code, konstantinvolosov@yandex.ru

Aleksandra K. Volosova, Candidate of Physical and Mathematical Sciences, Chief Analytical Department “Tramplin” LLC, Russian University of Transport (Obraztsova St. 9–9, Moscow, GSP-4, 127994, Russian Federation), ORCID, SPIN-code, alya01@yandex.ru

Mikhail I. Karlov, Candidate of Physical and Mathematical Sciences, Associate Professor of the Department of Mathematics, Moscow Institute of Physics and Technology (9, Institutsky Lane, GSP-4, Dolgoprudny, 141701, Russian Federation), SPIN-code, karlov.mipt@gmail.com

Dmitriy F. Pastukhov, Candidate of Physical and Mathematical Sciences, Associate Professor of Polotsk State University (Blokhin St. 29, Novopolotsk, 211440, Republic of Belarus), ORCID, SPIN-code, dmitrij.pastuhov@mail.ru

Yuriy F. Pastukhov, Candidate of Physical and Mathematical Sciences,Associate Professor of Polotsk State University (Blokhin St. 29, Novopolotsk, 211440, Republic of Belarus), ORCID, SPIN-code, pulsar1900@mail.ru

Contributions of the authors:

N.K. Volosova: ideas; formulation or evolution of overarching research goals and aims; writing — original draft preparation; software.

K.A. Volosov: supervision; methodology.

A.K. Volosova: translation; study of the history of the task; literature.

M.I. Karlov: formal analysis.

D.F. Pastukhov: visualization; validation.

Yu.F. Pastukhov: testing of existing code components.

***Conflict of Interest Statement:* the authors declare no conflict of interest.**

All authors have read and approved the final manuscript.

Об авторах:

Наталья Константиновна Волосова, аспирант Московского государственного технического университета им. Н.Э. Баумана (105005, Российская Федерация, г. Москва, ул. 2-я Бауманская, 5, стр. 1), ORCID, navalosova@yandex.ru

Константин Александрович Волосов, доктор физико-математических наук, профессор кафедры прикладной математики Российского университета транспорта (127994, ГСП-4, Российская Федерация, г. Москва, ул. Образцова, 9, стр. 9), ORCID, SPIN-код, konstantinvolosov@yandex.ru

Александра Константиновна Волосова, кандидат физико-математических наук, начальник аналитического отдела ООО «Трамплин» Российского университета транспорта (127994, ГСП-4, Российская Федерация, г. Москва, ул. Образцова, 9, стр. 9), ORCID, SPIN-код, alya01@yandex.ru

Михаил Иванович Карлов, кандидат физико-математических наук, доцент кафедры математики Московского физико-технического института (141701, ГСП-4, Российская Федерация, г. Долгопрудный, Институтский переулок, 9), SPIN-код, karlov.mipt@gmail.com

Дмитрий Феликсович Пастухов, кандидат физико-математических наук, доцент кафедры технологий программирования Полоцкого государственного университета (211440, Республика Беларусь, г. Новополоцк, ул. Блохина, 29), ORCID, SPIN-код, dmitrij.pastuhov@mail.ru

Юрий Феликсович Пастухов, кандидат физико-математических наук, доцент кафедры технологий программирования Полоцкого государственного университета (211440, Республика Беларусь, г. Новополоцк, ул. Блохина, 29), ORCID, SPIN-код, pulsar1900@mail.ru

Заявленный вклад авторов:

Н.К. Волосова: постановка задачи; написание черновика рукописи; формулировка идей исследования, целей и задач; разработка программного обеспечения.

К.А. Волосов: научное руководство; разработка методологии.

А.К. Волосова: перевод; изучение истории задачи; поиск литературы.

М.И. Карлов: формальный анализ.

Д.Ф. Пастухов: визуализация; валидация.

Ю.Ф. Пастухов: тестирование существующих компонентов кода.

Конфликт интересов: **авторы заявляют об отсутствии конфликта интересов.**

Все авторы прочитали и одобрили окончательный вариант рукописи.

Received / Поступила в редакцию 27.08.2025
Reviewed / Поступила после рецензирования 25.09.2025
Accepted / Принята к публикации 21.10.2025